Electronic Supplementary Material (ESI) for Materials Horizons.

Supporting Information

Understanding the charge dynamics in organic light-emitting diodes using convolutional neural network

Jae-Min Kim, Junseop Lim, and Jun Yeob Lee*

School of Chemical Engineering, Sungkyunkwan University

2066, Seobu-ro, Jangan-gu, Suwon, Gyeonggi-do, 16419, Republic of Korea

E-mail: leej17@skku.edu

* To whom correspondence should be addressed.

Supplementary Section 1

Supplementary Figures

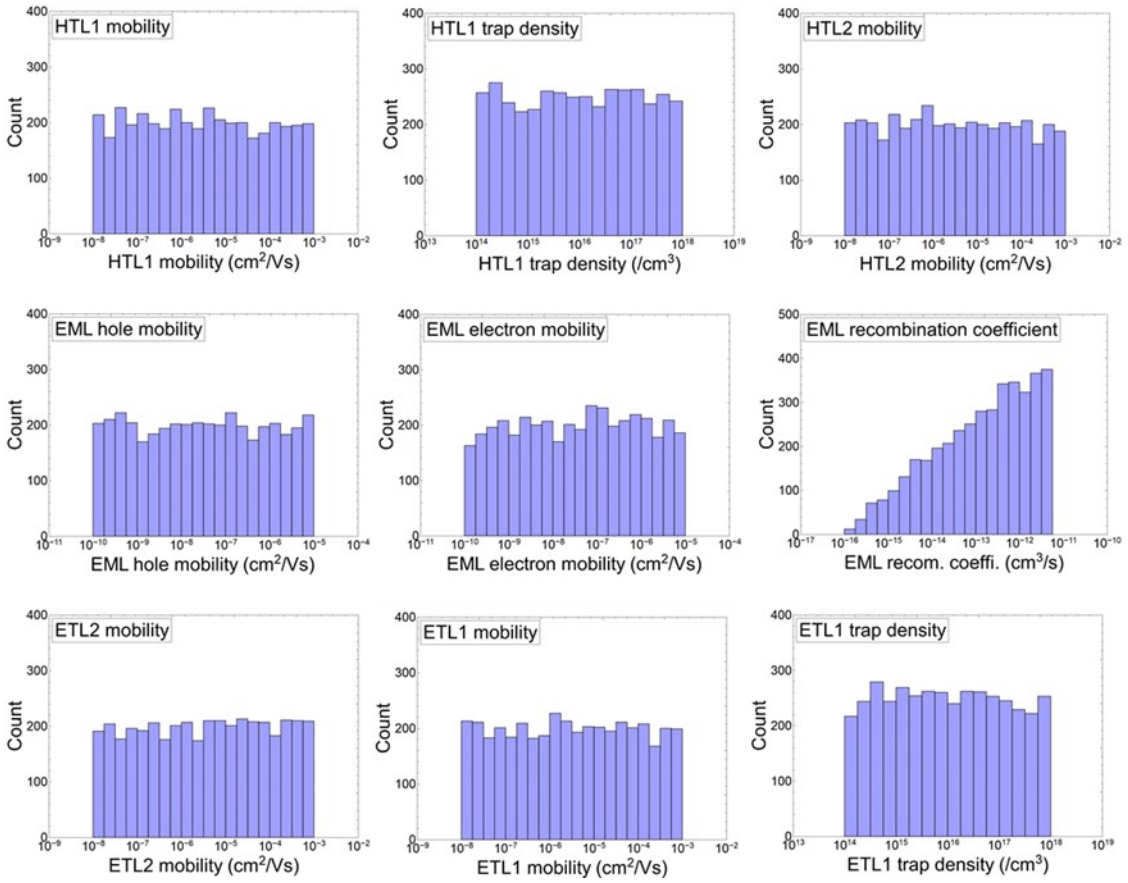

Figure S1. The distribution of the dataset as an output parameter.

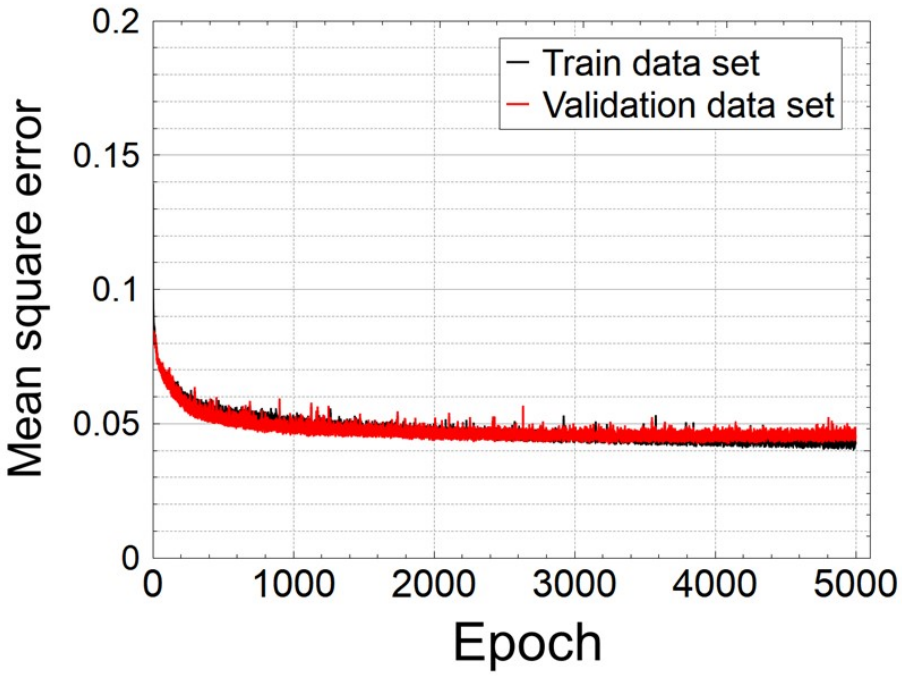

Figure S2. The learning curve of CNN-based neural network.

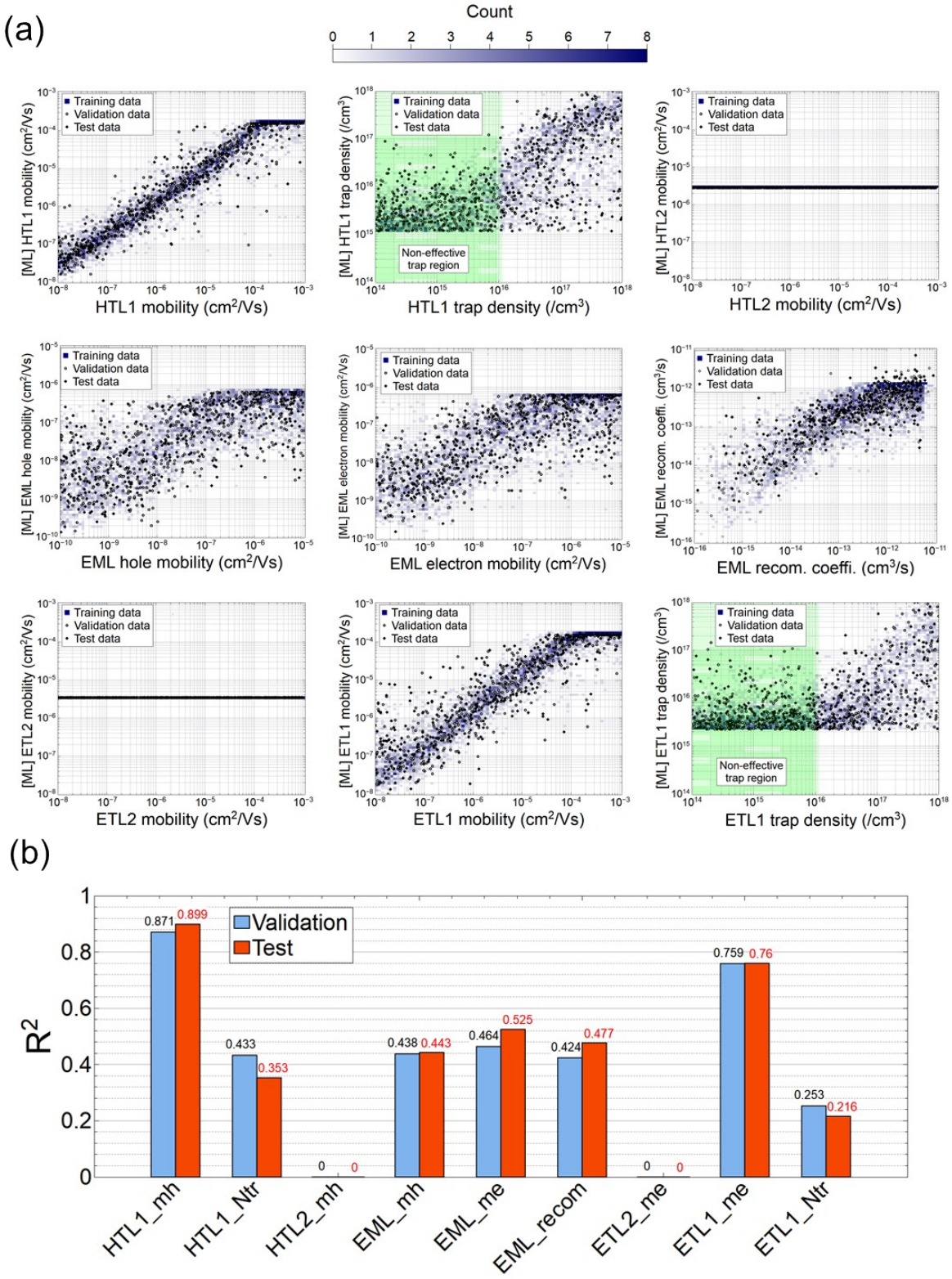

Figure S3. Prediction performance of the single task CNN models. (a) Distribution of predicted values for train/validation/test dataset. (b) R2 values of the CNN model applied in the validation and test dataset.

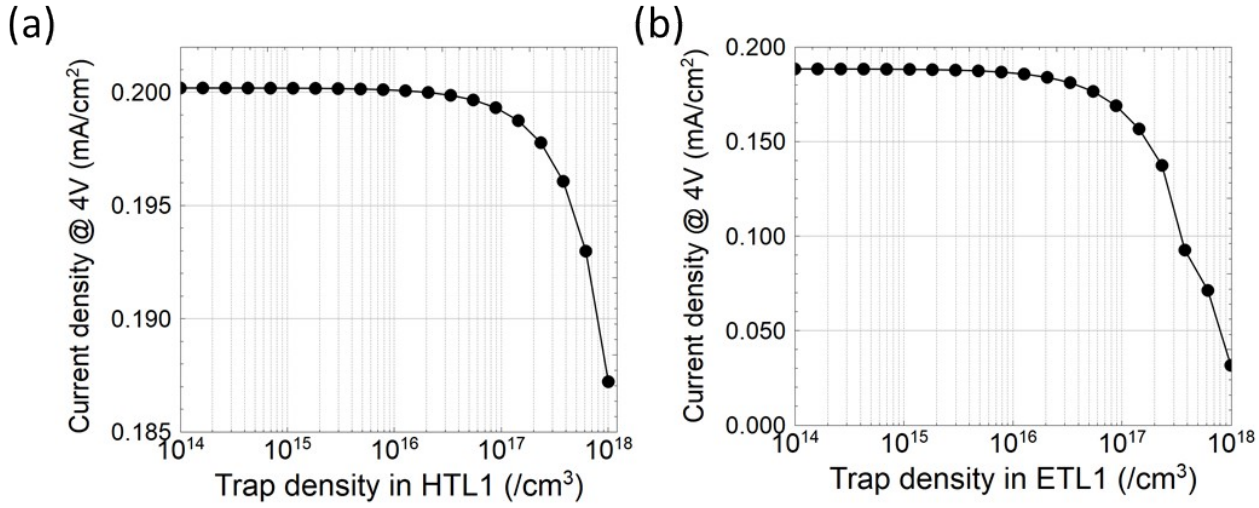

Figure S4. The current density at 4V according to various trap densities in HTL1 and ETL2 calculated by the drift-diffusion simulation.

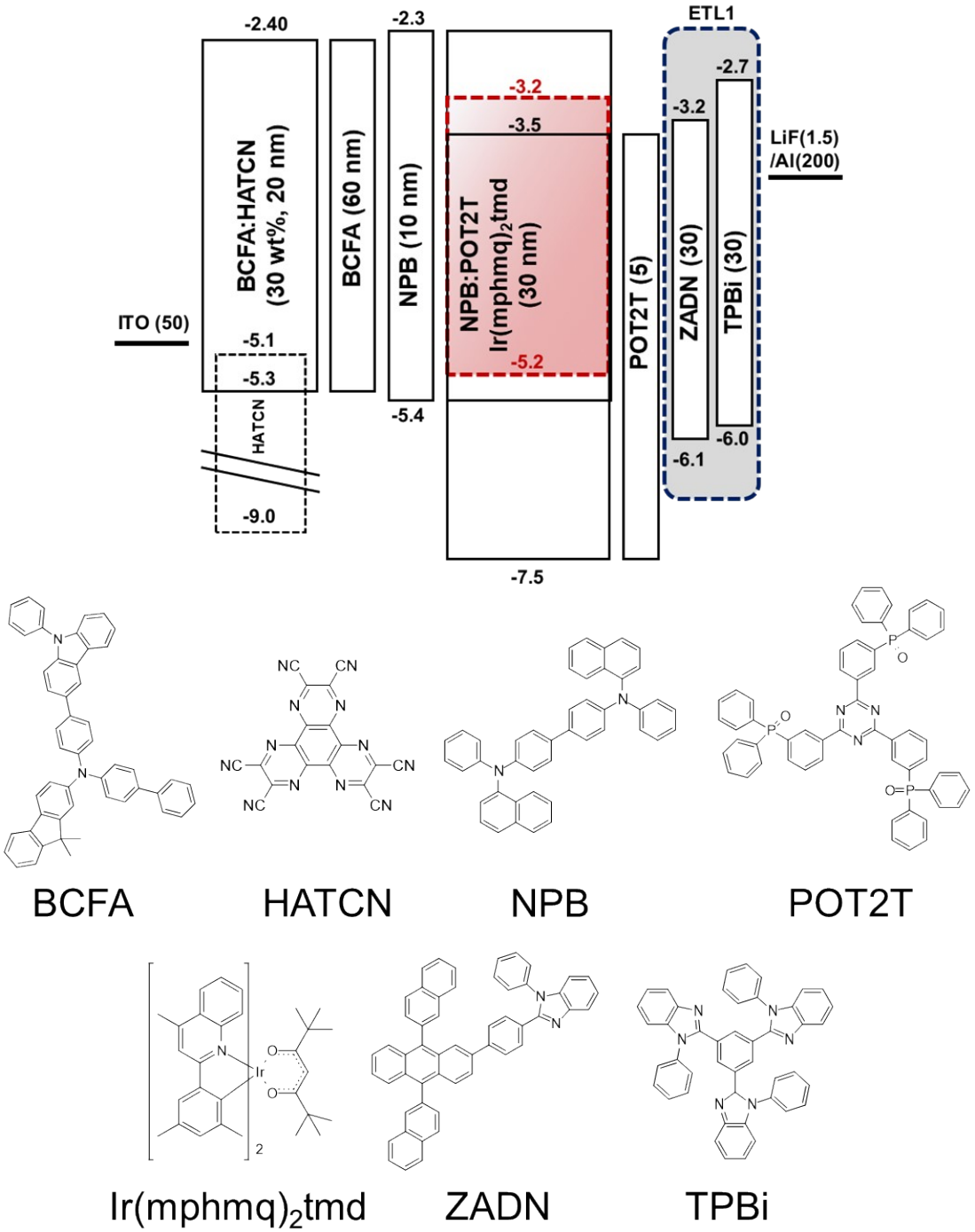

Figure S5. The device and molecular structures of red PhOLEDs.

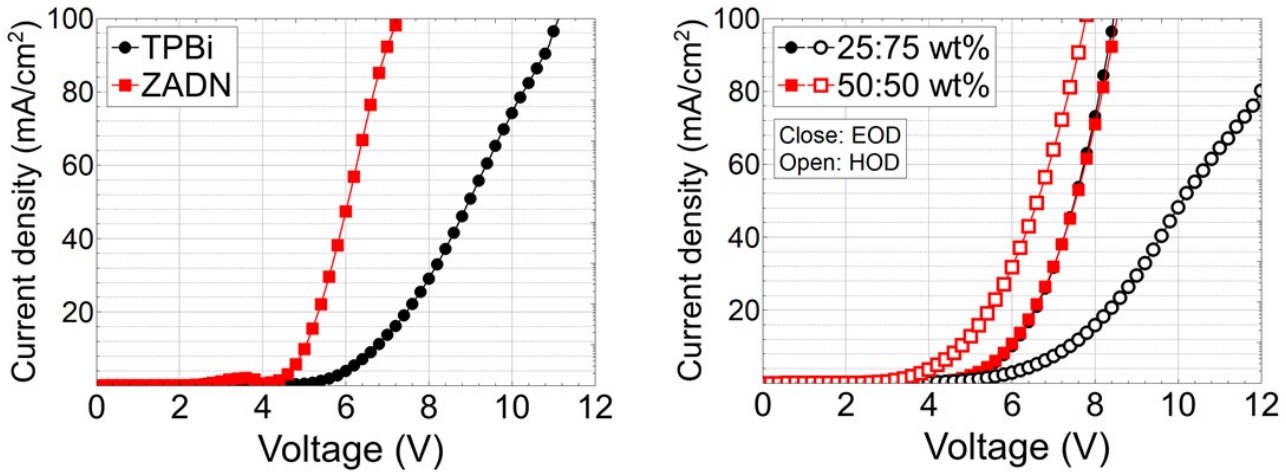

Figure S6. The current density-voltage characteristics of the unipolar charge devices.

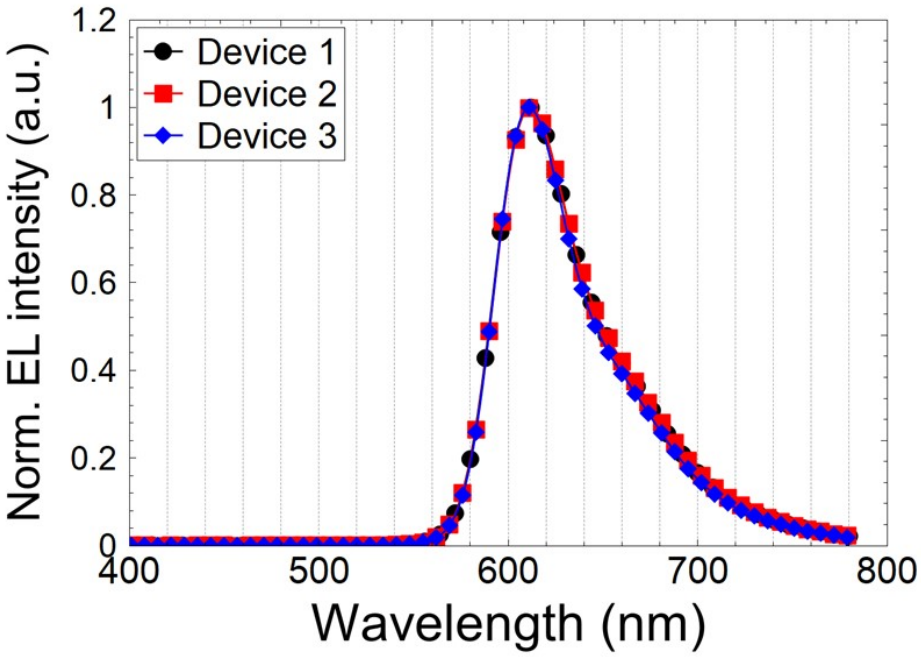

Figure S7. Electroluminescence spectra of red PhOLEDs.

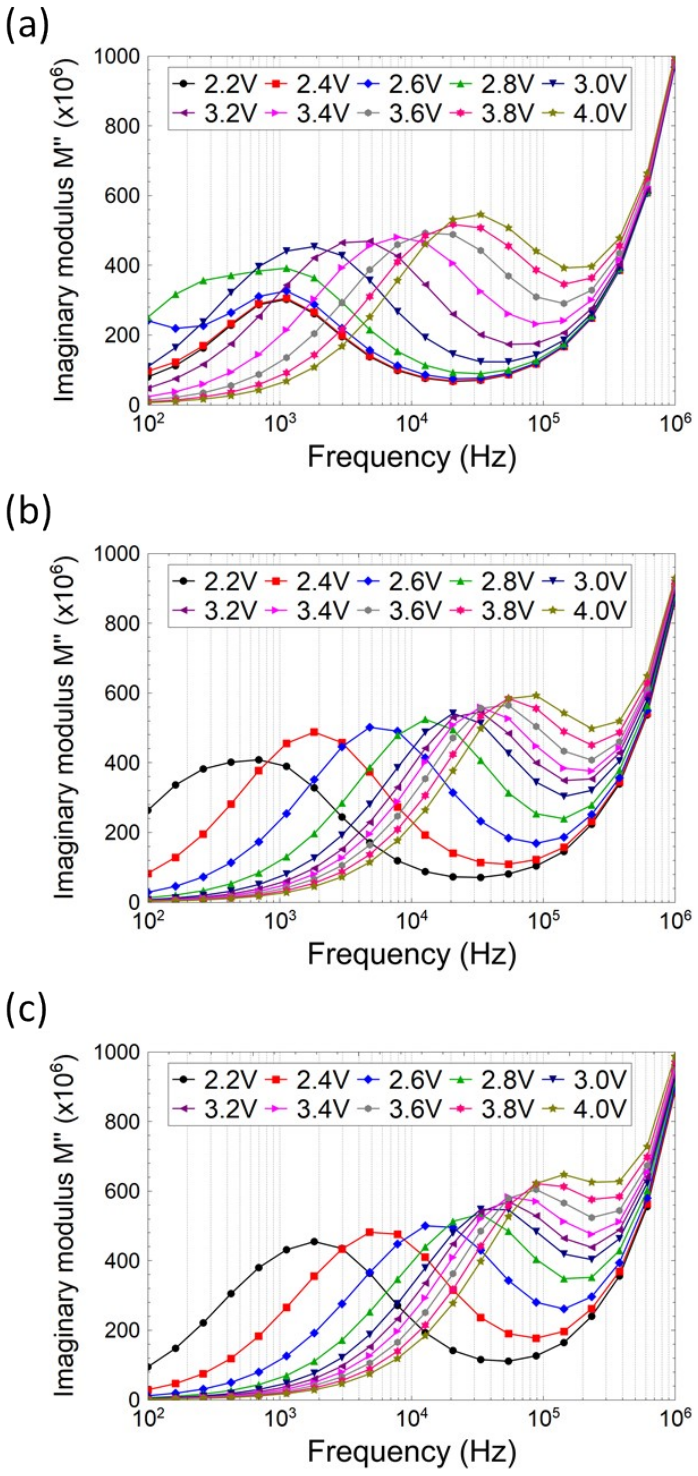

Figure S8. The modulus spectra of (a) device 1, (b) device 2, and (c) device 3.

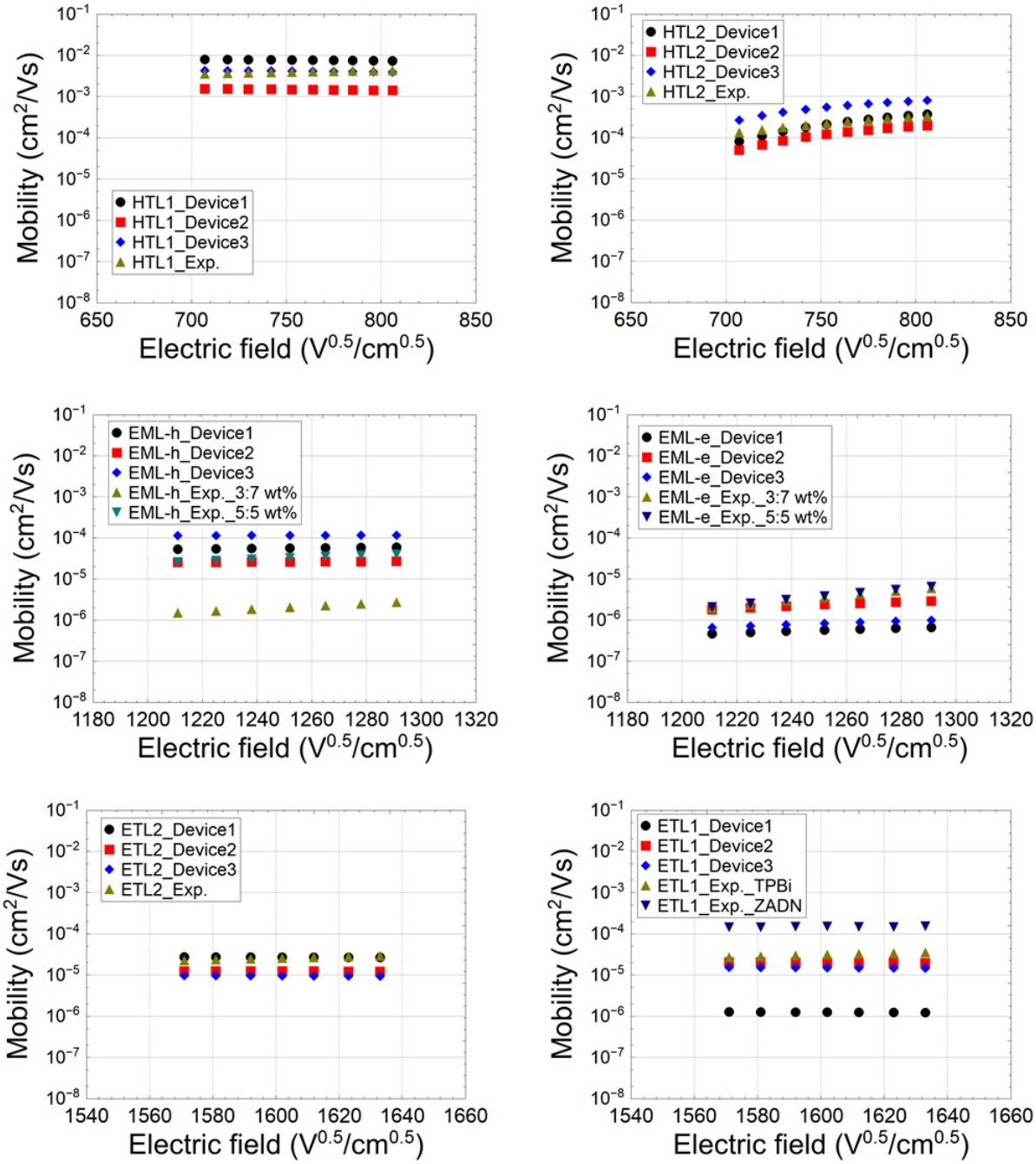

Figure S9. Predicted and experimental charge carrier mobilities of the organic layers used in the devices. The structures of the hole only devices for HTL1/HTL2/EML were ITO/HTL1 (50 nm)/Al, ITO/HTL1 (50 nm)/HTL2 (50 nm)/Al, and ITO/HTL1 (20 nm)/HTL2 (5 nm)/EML (30 nm)/HTL1 (10 nm)/Al. The structures of the electron only devices for ETL1/ETL2/EML were ITO/ETL1 (50 nm)/LiF/Al, ITO/ETL2 (50 nm)/ETL1 (50 nm)/LiF/Al, and ITO/ETL2 (10 nm)/EML (30nm)/ETL2 (5 nm)/ETL1 (30 nm)/LiF/Al.

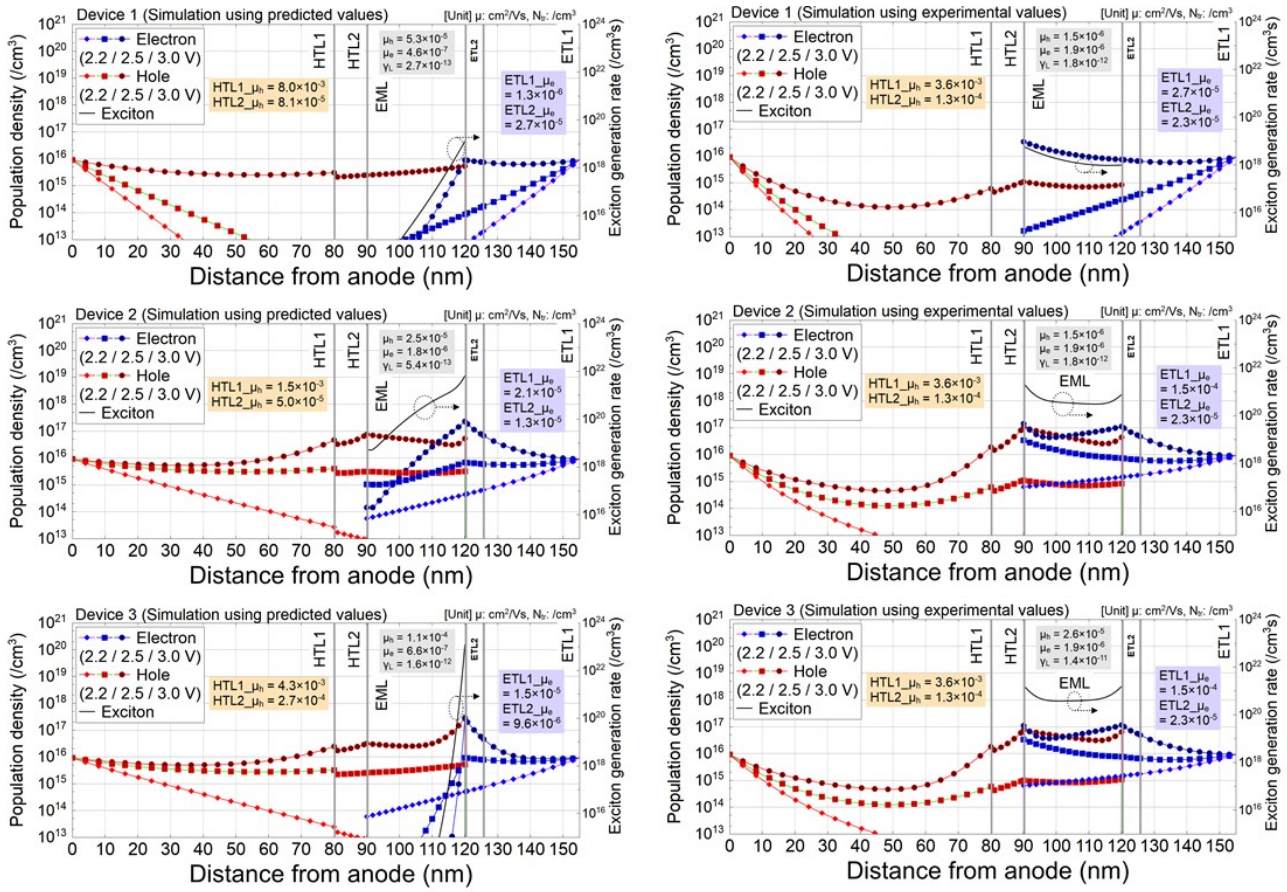

Figure S10. Spatial charge and exciton distributions for various operating voltages in red PhOLEDs simulated by the drift-diffusion modeling with predicted and experimental eletrical properties.

Supplementary Tables

Table S1. The boundaries of the output parameters in the dataset.

	Min. value	Max. value	Unit
HTL1 mobility	10^{-8}	10^{-3}	$cm^2\ V^{-1}s^{-1}$
HTL1 trap density	10^{14}	10^{18}	cm^{-3}
HTL2 mobility	10^{-8}	10^{-3}	$cm^2\ V^{-1}s^{-1}$
EML hole mobility	10^{-10}	10^{-5}	$cm^2\ V^{-1}s^{-1}$
EML electron mobility	10^{-10}	10^{-5}	$cm^2\ V^{-1}s^{-1}$
EML recom. coeff.	10^{-16}	10^{-11}	$cm^3\ s^{-1}$
ETL2 mobility	10^{-8}	10^{-3}	$cm^2\ V^{-1}s^{-1}$
ETL1 mobility	10^{-8}	10^{-3}	$cm^2\ V^{-1}s^{-1}$
ETL1 trap density	10^{14}	10^{18}	cm^{-3}

Table S2. The performance of the CNN based model according to the number of filters and nodes in the neural network. Dropout and learning rates were 0.5 and 0.001.

# of filters in cov layer1	# of filters in cov layer2	# of filters in cov layer3	# of nodes in dense layer	R^2	R^2_μHTL1	R^2_hEML	R^2_eEML	R^2_μETL1	MSE
5	5	5	50	0.424	0.856	0.354	0.330	0.617	0.053
10	10	10	50	0.401	0.832	0.344	0.262	0.604	0.055
20	20	20	50	0.505	0.830	0.454	0.451	0.720	0.048
40	40	40	50	0.514	0.834	0.522	0.460	0.716	0.047
60	60	60	50	0.523	0.847	0.502	0.484	0.724	0.047
80	80	80	50	0.485	0.795	0.448	0.483	0.737	0.049
60	60	60	20	0.421	0.713	0.400	0.372	0.637	0.054
60	60	60	100	0.536	0.846	0.518	0.529	0.766	0.047
60	60	60	200	0.534	0.878	0.511	0.552	0.788	0.048

Table S3. The performance of the CNN based model according to the drop rate. 60 filters and 100 nodes were used in the convolutional layers and the dense layer. The learning rate was 0.001.

Drop rate	R^2	R^2_μHTL1	R^2_hEML	R^2_eEML	R^2_μETL1	MSE
0.3	0.536	0.846	0.518	0.529	0.766	0.047
0.4	0.524	0.857	0.475	0.564	0.709	0.046
0.5	0.536	0.825	0.526	0.520	0.743	0.046
0.6	0.494	0.772	0.483	0.491	0.675	0.048

Table S4. The performance of the CNN based model according to the layer structure of the neural network. 60 filters and 100 nodes were used in the convolutional layers and the dense layer. Dropout and learning rates were 0.5 and 0.001.

Layer structure	R^2	R^2_μHTL1	R^2_hEML	R^2_eEML	R^2_μETL1	MSE
Conv / pooling	0.181	0.620	0.126	0.079	0.162	0.069
Conv / pooling / Conv	0.417	0.818	0.340	0.370	0.582	0.054
Conv / pooling / Conv / pooling / Conv	0.536	0.825	0.526	0.520	0.743	0.046
Conv / pooling / Conv / Conv	0.526	0.828	0.524	0.507	0.719	0.046

Table S5. The performance of the CNN based model according to the structure of the dense layer. 60 filters were used in the convolutional layers. Dropout and learning rates were 0.5 and 0.001.

Structure of dense layers	R^2	R^2_μHTL1	R^2_hEML	R^2_eEML	R^2_μETL1	MSE
100	0.536	0.825	0.526	0.520	0.743	0.046
100 / 100	0.511	0.849	0.488	0.440	0.718	0.047
100 / 100 / 100	0.432	0.849	0.331	0.337	0.700	0.054
100 / 50 / 50	0.513	0.840	0.492	0.502	0.711	0.047

Table S6. The performance of the CNN based model according to the learning rate. 60 filters and 100 nodes were used in the convolutional layers and the dense layer. Dropout rate was 0.5.

Learning rate	R^2	R^2_μHTL1	R^2_hEML	R^2_eEML	R^2_μETL1	MSE
0.002	0.465	0.805	0.413	0.350	0.696	0.050
0.001	0.536	0.825	0.526	0.520	0.743	0.046
0.0005	0.528	0.831	0.514	0.487	0.754	0.046
0.0001	0.516	0.855	0.462	0.490	0.713	0.047

Supplementary Section 2

Supplementary information of the drift-diffusion simulation

The charge transport in organic light-emitting diodes was described by the electric field-driven transport (drift current) and the differential concentration-driven transport (diffusion current) as following equations.[1–4]

$$\frac{\varepsilon_0 \varepsilon_r \partial^2 \varphi(x,t)}{q \quad \partial x^2} = p(x,t) - n(x,t) + N_D + N_A + \sum \rho_t(x,t)$$

$$\frac{\partial p(x,t)}{\partial t} = \frac{1}{q}\frac{\partial}{\partial x}\left[-\frac{\mu_p kT \partial p(x,t)}{q \quad \partial x} - \mu_p p(x,t)\frac{\partial \varphi(x,t)}{\partial x}\right] + R(x,t)$$

ε_0, ε_r, q, $\varphi(x,t)$, $p(x,t)$, $n(x,t)$, N_D, N_A, ρ_t, and R are the vacuum permittivity, dielectric permittivity, electronic charge, electric potential, hole density, electron density, ionized donor density, ionized acceptor density, trap charge, and recombination rate, respectively. To mathematically realize the charge transport in the density of states in the organic semiconductors, the combination of mobility and trap distribution was adopted in the simulation. The number of the trapped holes with the trap density $N_t(E)$ and trap distribution function f_t was described by

$$\rho_t(x,t) = \int \left(1 - f_t(E,x,t)\right) N_t(E) dE$$

The trap distribution was assumed as an exponential distribution in the bandgap energetic region. The impedance in the small perturbation condition was derived by introducing time-dependent oscillation terms to the steady-state parameters as follows.[1,5–7]

$$n(x,t) = n(x) + \tilde{n}(x) e^{i\omega t}$$

$$p(x,t) = p(x) + \tilde{p}(x) e^{i\omega t}$$

$$\phi(x,t) = \phi(x) + \tilde{\phi}(x) e^{i\omega t}$$

$\tilde{n}(x)$, $\tilde{p}(x)$, and $\tilde{\phi}(x)$ was assumed as a small amplitude in the perturbation function and ω is the angular frequency. The device structure of OLED is set to ITO / HTL1 (80 nm) / HTL2 (10 nm) / EML (30 nm) / ETL2 (5 nm) / ETL1 (30 nm) / Al. The injection barrier at the organic/metal electrodes interfaces was assumed to be 0.3 eV. The output physical values in the datasets, which were HTL1 hole mobility, HTL1 trap density, HTL2 mobility, EML hole mobility, electron mobility, recombination coefficient, ETL2 mobility, ETL1 electron mobility, and ETL1 trap density, were normalized to have the values from 0 to 1 and utilized in the machine learning framework for enhancing the predictivity. The physical parameters were randomly generated in the log-scale to uniformly distribute the values in the log-scale dimension. For the modulus spectra, the normalization of the modulus intensity for each case was performed based on the maximum modulus value in whole datasets rather than the maximum value of each case because relative intensity in the modulus spectra was correlated with the capacitor components (charge storage or accumulation) in the charge dynamics.

References

[1] J. Staudigel, M. Stößel, F. Steuber, J. Simmerer, *J. Appl. Phys.* **1999**, *86*, 3895–3910.

[2] B. Ruhstaller, S. A. Carter, S. Barth, H. Riel, W. Riess, J. C. Scott, *J. Appl. Phys.* **2001**, *89*, 4575–4586.

[3] J. -M. Kim, C. H. Lee, J. J. Kim, *Appl. Phys. Lett.* **2017**, *111*, 75307.

[4] C. H. Lee, J. H. Lee, K. H. Kim, J. J. Kim, *Adv. Funct. Mater.* **2018**, *28*, 1–8.

[5] N. D. Nguyen, M. Schmeits, *Phys. Status Solidi A* **2006**, *203*, 1901–1914.

[6] E. Knapp, B. Ruhstaller, *Appl. Phys. Lett.* **2011**, *99*, 37–40.

[7] E. Knapp, B. Ruhstaller, *Opt. Quantum Electron.* **2011**, *42*, 667–677.